

Journal of Materials Chemistry C

Accepted Manuscript



This is an *Accepted Manuscript*, which has been through the Royal Society of Chemistry peer review process and has been accepted for publication.

Accepted Manuscripts are published online shortly after acceptance, before technical editing, formatting and proof reading. Using this free service, authors can make their results available to the community, in citable form, before we publish the edited article. We will replace this *Accepted Manuscript* with the edited and formatted *Advance Article* as soon as it is available.

You can find more information about *Accepted Manuscripts* in the [Information for Authors](#).

Please note that technical editing may introduce minor changes to the text and/or graphics, which may alter content. The journal's standard [Terms & Conditions](#) and the [Ethical guidelines](#) still apply. In no event shall the Royal Society of Chemistry be held responsible for any errors or omissions in this *Accepted Manuscript* or any consequences arising from the use of any information it contains.

Chitosan-Based Biopolysaccharide Proton Conductors For Synaptic Transistors On Paper Substrates

Guodong Wu^{1,2*}, Jin Zhang², Xiang Wan^{1,2}, Yi Yang¹, Shuanghe Jiang¹

1) School of Electronic Science and Engineering, Nanjing University, Nanjing 210093, People's Republic of China

2) Ningbo Institute of Material Technology and Engineering, Chinese Academy of Sciences, Ningbo 315201, People's Republic of China

Abstract

Chitosan is a natural biopolymer and has been widely used for bio- and medical-materials. In this letter, with protonic acid doping, chitosan-based biopolysaccharide proton conductors were prepared with high proton conductivity of 6×10^{-3} S/cm at room temperature and were first used for fabricating synaptic transistors on paper substrates. Based on the movement of protons with pulse voltage response within the chitosan dielectrics in an coplanar-gate transistor configuration, the paper synaptic transistors could be successfully used as artificial synapses for emulating biological synaptic functions. Short-term plasticity behaviors, including paired-pulse facilitation, dynamic filtering and spatiotemporally correlated signal processing were mimicked. Our results strongly demonstrate these biopolysaccharide gating synaptic transistors proposed here are not only important for building cheap and biological friendly artificial neuron networks, but also are interesting for realizing intelligent biomaterials.

Key Words: Chitosan-based proton conductors, Synaptic transistors, Paper substrates

* Corresponding author. Tel./Fax: +86 25 8359 6644.

E-mail address: wuguodong110110@163.com

Introduction

The synapses are the crucial connective parts between neurons for realizing functions of information transmission, signal processing, memory and learning in human brain.¹⁻³ Synaptic strength or synaptic weight, as a measurement of synapse efficacy in establishing the connection between pre-synaptic and post-synaptic neurons, can be precisely adjusted by the concentrations of ionic species (e.g., Ca^{2+} , Na^+ , and K^+ , etc).⁴⁻⁵ The ion excitatory postsynaptic current (Excitatory Postsynaptic Current, EPSC), as the basic representation of synaptic strength, is a temporary current caused by the flow of ions into the post-synaptic cell as a result of the pre-synaptic neuron spike.⁶⁻⁷ In order to build for artificial neural network and intelligent computer, realization of physical device with the functions of a biological synapse is of great importance.⁸⁻¹¹ Previously, silicon complementary metal-oxide-semiconductor (CMOS) chips have been designed to emulate the brain behaviors. However, this approach is limited to small systems because it takes at least seven silicon transistors to build an electronic synapse.¹² It is essential to develop a nanoscale and low power device in order to scale neuromorphic circuits towards the level of the human brain. These features have prompted the research on two-terminal memristors or memory devices as the hot candidates in artificial synapses fields for their analogous structure, function and physics chemical mechanism to biological synapses.¹³⁻¹⁵ For example, short-term plasticity and long-term potentiation have been mimicked in a single Ag_2S memristor.¹⁶ Most recently, three-terminal electrolyte gating transistors have been creatively designed as artificial synapses for emulating

biological synaptic functions.¹⁷⁻¹⁹ Based on the mobile hydrogen ions within the PEG polymer dielectrics in a CNT-based transistor configuration, EPSC, dynamic logic, learning and memory functions of a biological synapse were demonstrated in these CNT-based synapses.¹⁷ These electrolyte gating synaptic transistors greatly enriched bionic electronic synapses in terms of the limitations of materials and devices. It provided a new way to realize artificial neural networks and intelligent computer.

Chitosan is a biodegradable, biocompatible, nontoxic, and low-cost polymer, which shows many interesting properties, such as wound healing, antibacterial activity, and binding in tissue.²⁰ Therefore, chitosan has been widely used for bio- or medical-materials, such as a tissue engineering material, surgical tape, and artificial skin.²¹⁻²³ Besides, due to its high proton conductivity by acid doping, chitosan has also attracted much attention as solid electrolyte membrane in fuel cells and low-voltage thin-film transistors.²⁴⁻²⁶ However, chitosan as bionic synaptic material has been no reported. Applications of biopolymers in bionic synaptic devices are not only important for cheap and biological friendly bionic electronics but also interesting for realizing intelligent biomaterials. Meantime, for fabricating bionic electronics, substrate materials are of great important. Compared to other flexible substrates (e.g. plastic substrates), paper is an intriguing alternative to fulfill low-cost and biological friendly demand, because it is one of the most abundant materials and a renewable resource.²⁷⁻²⁹ Thus, in this work, chitosan-based biopolysaccharide proton conductors were used as gate dielectrics for fabricating coplanar-gate synaptic transistors on paper substrates. Based on the movement of protons by pulse voltage response within

the chitosan dielectrics in an coplanar-gate transistor configuration, the paper synaptic transistors here can be successfully used as artificial synapses for mimicking biological synaptic plasticity behaviors, including paired-pulse facilitation, dynamic filtering and spatiotemporally correlated signal processing.

Experimental

Paper substrates used for coplanar-gate chitosan gating synaptic transistors were photo papers for ink-jet printing. The front of the photo paper has a absorbent coating, while the back is smooth and has no absorbent coating. The synaptic transistors here were fabricated onto the smooth back of the photo paper. The schematic diagram of coplanar-gate chitosan gating synaptic transistors on the paper substrate is shown in Fig.1(a). First, chitosan solution (4 wt% in acetic acid) was directly drop-casted onto a paper substrate and dried in air to form a film. Then, the patterned indium-zinc-oxide (IZO) layer films used for source/drain/coplanar gate electrodes (size: $150\ \mu\text{m}\times 1000\ \mu\text{m}$) were deposited on the chitosan-based proton conductor film with a nickel shadow mask by radio frequency (RF) magnetron sputtering in a vacuum pressure of 0.5 Pa. A thin IZO channel can be self-assembled between the IZO source/drain electrodes due to the diffraction effect.³⁰ The channel length is $\sim 80\ \mu\text{m}$ and the channel width is $\sim 1000\ \mu\text{m}$. Field-emission scanning electron microscope (FESEM, Hitachi S-4800) was used to analyze the cross-sectional images of chitosan-based proton conductor films. Solartron 1260 impedance analyzer was used to measure complex impedance of chitosan-based proton conductor films with sandwich structure (N-type Si/chitosan-based proton conductor/IZO). Keithley 4200 semiconductor parameter

analyzer was used to test the electrical characteristics. Both the complex impedance analysis and electrical characteristics were performed at room temperature in air ambient at the relative humidity of 70%.

Results and discussion

Fig. 1(b) shows cross-sectional SEM image of the chitosan-based proton conductor film on a N-type Si substrate. Loose microstructure with nanopores is observed, which is favor for proton migration.³¹ The thickness is estimated to be ~ 6 μm . Inset in Fig. 1(b) is the cross-sectional SEM image of the chitosan-based proton conductor film on a smooth back of the photo paper. It can be seen the chitosan film is basically homogenous in the nanoscale range. The chitosan-paper interface is obvious, indicating the paper doesn't absorb the chitosan. Fig. 1(c) shows the photo of the bent IZO-based synaptic transistor arrays gated by the chitosan-based proton conductor on a paper substrate, which demonstrates a good flexible characteristic.

As we known, the ionic conductivity of chitosan in natural state is as low as 10^{-9} S/cm^{-1} though abundant amino and hydroxyl functional groups exist in chitosan. These groups graft on the polysaccharide framework with strong chemical bonds and they can not work as the mobile ions. However, when the chitosan is doped by acetic acid, the protonation process occurs in chitosan molecules.³² As shown in Fig. 2(a), the proton (H^+) is dissociated from acetic acid and results free amino group in the chitosan backbone in protonation ($-\text{NH}_2 + \text{HAc} \leftrightarrow -\text{NH}_3^+ + \text{Ac}^-$). At the same time, the water molecules absorbed in the chitosan chains can form hydrogen-bond sites for the proton transferring from amino groups to water molecules ($-\text{NH}_3^+ + \text{H}_2\text{O} \leftrightarrow -\text{NH}_2 +$

H_3O^+).²⁵ In order to evaluate the proton conductivity of protonic acid doping chitosan film, the Cole-Cole plot was characterized in Fig. 2(b). Impedance spectroscopy data are collected as real ($\text{Re } Z'$) and imaginary ($\text{Im } Z''$) components of the complex impedance. The impedance real value (R) of 120Ω is obtained with the impedance imaginary value equal to zero. The conductivity (σ) could be obtained from the relation below:³³

$$\sigma = \frac{D}{(R - R_0)A}$$

where D , A and R_0 are the thickness of chitosan-based proton conductor film, electrode surface area, and the resistance of the electrodes, respectively. The thickness D is $\sim 6 \mu\text{m}$, A is $\sim 1.5 \times 10^{-3} \text{ cm}^2$, while R_0 is measured to be $\sim 30 \Omega$. Therefore, the conductivity (σ) is estimated to be $\sim 6 \times 10^{-3} \text{ S/cm}$, indicating that the chitosan-based proton conductor film shows high proton conductivity at room temperature. Here, we should point out the water absorption can create plenty of proton-conducting hydrogen-bond chains which serve as proton wires for proton transfer to occur, as shown in Fig. 2(c), protons originated from the protonated amino groups can move along the hydrated molecule hydrogen-bond network following the Grotthum mechanism.³⁴ Abundant mobile protons are essential for high proton conductivity in our chitosan-based proton conductor film. By using chitosan-based proton conductors as gate dielectrics, flexible paper coplanar-gate synaptic transistors were fabricated, as shown in Fig.1(a). The IZO films were at the same time utilized as gate/source/drain electrodes that all can be deposited through one mask and in one-step self-assembly. The reasons for choosing IZO as gate/source/drain electrodes are based on the

following two points: First, IZO is an amorphous oxide that allows for high mobility and controllable conductivity, which permits it to be used both as a transparent semiconductor or conductor, and so to be used both as active and source/drain layers of TFTs.³⁵ Second, the work function of tungsten probes (semiconductor parameter analyzer) is ~4.54-4.91 eV and the work function of IZO is ~5.1 eV. Therefore the barrier height is low. The IZO film with high doping concentration ($10^{18}/\text{cm}^3$, measured by hall measurement) is also conductive.³⁶ Thus, good ohmic contact can be achieved between gate electrodes (IZO) and tungsten probes.

Biological synapses are the functional connections between biological neurons, Its schematic digram is shown in Fig. 3 (a). In our brain, signal processing, memory and learning functions are all achieved by modulating the ion flow in neurons and synapses. The ionic fluxes through the ion channels localized at synapses result in the movements of neurotransmitters, modulating the synapse efficacy in establishing the relationship between pre-synaptic neurons and the post-synaptic neurons.³⁷ The pre-synaptic neuron spikes would trigger EPSC in biological systems.⁶⁻⁷ Although two-terminal memristors have been reported to be good candidates for artificial synapse applications, two-terminal memristors shows similarities to ‘point-to-point’ connected synapses. As an alternative, three-terminal transistors show similarities to ‘point-to-line’ connected dendrite synapses. These kinds of three-terminal devices are also interesting for artificial synapses. In our case, the coplanar gate electrode and channel layer could be regarded as pre-synaptic neuron and post-synaptic neuron, respectively, while the protons within the chitosan films can be used as the

neurotransmitters and the channel conductance is regarded as the synaptic weight, as shown in Fig. 3 (b). Proton migration triggered by the pre-synaptic spikes applied on the IZO gate electrode results in the establishment of the inter-connections between the pre-synaptic neuron and the post-synaptic neuron. Such process is analogue to the spike modulated movement of the neurotransmitters in biological synapse, modulating the synapse efficacy in establishing the relationship between pre-synaptic neurons and the post-synaptic neurons.

To test the synaptic response of such synaptic transistor, selecting gate pulse voltage is important. In previous studies, a high gate pulse (>3 V) voltage can easily trigger electrochemical proton doping process in the IZO channel layer, which is not conducive to short-term plasticity behaviors emulation.³⁸ However, much low gate pulse (<0.5 V) voltage may show a low signal to noise ratio. Therefore, in order to insure both high signal to noise ratio and low consuming energy dissipation, a pre-synaptic spike (0.5 V, 10 ms) was applied on the gate electrode, as shown in Fig. 3(c). The post-synaptic current is measured with a constant drain-source bias of 0.6 V. As shown in Fig. 3(d), the pre-synaptic spike triggers an EPSC above the resting current (~ 3.2 nA). EPSC reaches a peak value of ~ 42.6 nA at the end of the spike, and gradually decays back to the resting current. Such EPSC behaviors are quite similar to an EPSC process in a biological excitatory synapse. A simple estimate of energy consumption can be made by multiplying the reading voltage with the current flowing across the channel and the programming pulse width. The average energy consumption to trigger an EPSC is estimated to be ~ 26 pJ/spike, which is significantly

lower than the energy consumption by conventional CMOS circuit (~ 900 pJ/spike).¹⁷ At present, the size of these synaptic transistors fabricated by simple on-shadow-mask self-assembly method is large. However, it could be scaled down to sub-micrometer scale by photolithography technology. Such scaling can further reduce the energy dissipation down to 1.0 pJ/spike and increase the number of unit area. Low energy dissipation and high density integration is the aim for neuromorphic system application. In the synaptic transistor proposed here, protons in lateral movement in chitosan films play an essential role to trigger EPSC. When a pre-synaptic spike is applied on the gate electrode, positive charged protons are driven laterally towards and accumulate at the chitosan/gate electrode interface, which attracts free electrons in the IZO channel and increases the post-synaptic current through the IZO channel, as shown in Fig.3(b). After pre-synaptic spike, protons gradually drift back to their equilibrium positions in chitosan-based proton conductor, therefore, the electron concentration in the IZO channel and the post-synaptic current decrease.

Paired pulse facilitation (PPF) is a common form of short-term synaptic plasticity in biological synapses and essential to decode temporal information in auditory or visual signals. In many systems, a single synaptic activation will facilitate a subsequent synaptic response. When a pre-synapse receives two spikes in a rapid succession, the postsynaptic response will commonly be larger for the second than for the first spike. With the decreasing inter-spike duration time, a greater postsynaptic response or a higher PPF would be obtained.³⁹⁻⁴⁰ The synaptic transistors proposed here could also process temporally correlated spikes and generate temporal analog

logic such as PPF. The PPF in our synaptic transistor is demonstrated by applying two successive pre-synaptic spikes (0.5 V, 10 ms) with an inter-spike interval, Δt_{pre} , ranging between 10 ms and 2000 ms. Fig. 4 (a) shows the EPSC triggered by the second pre-synaptic spike is larger than the EPSC by the first spike with the inter-spike duration of 200 ms. The scheme of the EPSCs triggered by a pair of temporally correlated pre-synaptic spikes in our synaptic transistor is shown in the inset of Fig.4 (b). PPF index defined as the ratio of the amplitudes between the second EPSC and the first EPSC is plotted versus Δt_{pre} , as shown in Figure 4(b). The PPF index reaches the maximum value of ~180 % at $\Delta t_{\text{pre}} = 10$ ms and gradually decreases with increasing Δt_{pre} . After the first spike, the protons within chitosan-based proton conductor would drift back to their equilibrium positions due to the concentration gradient. If the inter-spike interval is very short, the protons triggered by the first spike will still partially reside near the IZO channel. Thus, the protons triggered by the second spike are augmented with the residual protons triggered by the first spike. The longer Δt_{pre} would induce less residual protons near IZO channel and result in lower value of A_2/A_1 . Thus, the PPF and the short-term synaptic plasticity are mimicked in our coplanar-gate chitosan gating synaptic transistors. The results show that the synaptic transistors here can be well regarded as artificial synapses to simulate biological synapses with excited stimulation response and short-term synaptic plasticity.

In brain nervous system, synaptic efficacy can increase (synaptic facilitation) or decrease (synaptic depression) markedly within milliseconds after the onset of

specific temporal patterns of activity.⁴¹ Due to the short-term synaptic depression or facilitation, synapses could also act as dynamic filters for information transmission depending on the signal frequencies. The short-term synaptic depression contributes to low-pass temporal filtering and the short-term synaptic facilitation contributes to high-pass temporal filtering.⁴² The above PPF results demonstrated a higher PPF index value is obtained with the shorter Δt_{pre} , therefore, in our synaptic transistor, a high-pass filter could be realized. The temporal filtering function was tested by applying the stimulus train consisted of 10 stimulus spikes (0.5 V, 10 ms) at each frequency on the coplanar gate. $V_{\text{ds}}=0.5$ V is applied to the source and drain electrodes for EPSCs measurements. Figure 5 (a) shows the EPSC responses of our device to the stimulus train with different frequencies. For the frequency of the stimulus train is 1.0 Hz, the peak value of the EPSC keeps at ~ 36 nA even after 10 spikes. When the frequency of the stimulus train is increased, the peak values of the measured EPSCs increase obviously. Figure 5 (b) shows the frequency dependent gain defined as the ratio of the amplitudes between the tenth EPSC (A_{10}) and the first EPSC (A_1). The gain increases from ~ 1.0 to ~ 10.6 when the stimulus frequency changes from 1.0 Hz to 100 Hz, which indicates that our synaptic transistor can act as the dynamic high-pass filter for information transmission. It is expected the gain (A_{10}/A_1) increases when the stimulus frequency changes from low frequency to high frequency. In brain nervous system, short-term synaptic plasticity is widely believed to play an important role in synaptic computations and information processing. When the outer stimulus (e.g. visual stimulus or auditory stimulus) interval time is longer,

the initial memories in the brain could be forgotten, while the stimulus interval time is shorter, the successive stimulates induce a short-term memory in the brain. In the synaptic transistor, the gate pulse voltage is as the outer stimulus, the gain (A_{10}/A_1) is as the memory strength and the frequency is as stimulus interval time, therefore, the gain (memory strength) increases when gate pulse frequency changes from low frequency (long stimulus interval time) to high frequency (short stimulus interval time). The high-pass temporal filtering mimicked here is meaningful for neuromorphic computations and artificial neural network.

The spatiotemporally correlated stimuli from different neurons would trigger a post-synaptic neuron to establish a dynamic logic. In order to mimicking the biological spatiotemporal dynamic logic, chitosan gating synaptic transistor with two coplanar gates is designed, as shown in Fig. 6 (a). Fig. 6 (b) shows the schematic diagram of spatial summation testing. Two pre-synaptic spikes with an inter-spike interval ($\Delta t_{\text{pre2-pre1}}$) are applied on pre-synapse **1** and pre-synapse **2** respectively, the two EPSCs will be summed in the post-synapse, which is a dynamic analog function of time and $\Delta t_{\text{pre2-pre1}}$. The responses of the post-synapse are measured with a constant V_{ds} of 0.5 V. Pre-synaptic spike (0.5 V, 20 ms) on pre-synapse **1** will trigger an EPSC **1** and pre-synaptic spike (1.0 V, 20 ms) on pre-synapse **2** will trigger an EPSC **2**, as shown in Fig. 6 (c). Figure 6(d) illustrates the amplitude of the EPSC as a function of the inter-spike interval $\Delta t_{\text{pre2-pre1}}$. When $\Delta t_{\text{pre2-pre1}}=0$, the EPSC **1** and EPSC **2** are triggered simultaneously, therefore the amplitude of the EPSC in the post-synapse reaches the maximum value. When EPSC **1** from pre-synapse **1** is triggered earlier

than EPSC **2** from pre-synapse **2** ($\Delta t_{\text{pre2-pre1}} > 0$), protons triggered by pre-synaptic spike **2** will migrate to interface region later than that triggered by pre-synaptic spike **1**. Therefore, the amplitude of EPSC at $t=0$ is equal to the peak amplitude of EPSC **1**. When EPSC **1** from pre-synapse **1** is triggered later than EPSC **2** from pre-synapse **2** ($\Delta t_{\text{pre2-pre1}} < 0$), the protons triggered by pre-synaptic spike **1** will be augmented with that triggered by pre-synaptic spike **2**. When $\Delta t_{\text{pre2-pre1}}$ is increased, more and more protons triggered by pre-synaptic spike **2** will drift back to their equilibrium position. Thus, the number of protons accumulated at the interface will decrease. Therefore, EPSC value at $\Delta t=0$ will decrease gradually as a function of $\Delta t_{\text{pre2-pre1}}$. Namely, the effects of the pre-synaptic spike on pre-synapse **2** are getting less important. Here, it is worth mentioned that such coplanar-gate synaptic transistors is favor for the construction for an artificial synapse network with many different pre-synaptic inputs by simply adding other coplanar gates. Therefore, our coplanar-gate chitosan gating synaptic transistors are very interesting for the realization of future artificial synapse network and neuromorphic computing systems. Of course, as the flexible paper synaptic transistors, measurements of synaptic performance on bent state are important for their practical flexible applications. The research, including the influence of bent times or bent angle on synaptic emulations by these paper synaptic transistors, will be systematically studied in our future works.

Conclusions

In summary, chitosan doped by acetic acid demonstrated high proton conductivity of 6×10^{-3} S/cm at room temperature and were first used for fabricating

synaptic transistors on paper substrates with simple coplanar-gate configuration. Based on the strong proton lateral migration ability with pulse voltage response in the chitosan-based proton conductor film, the paper synaptic transistors could be successfully mimicking biological synaptic functions, including excitatory postsynaptic current, paired-pulse facilitation, dynamic filtering and spatiotemporally correlated signal processing. Our results strongly demonstrate such biopolysaccharide gating synaptic transistors are not only important for building cheap and biological friendly artificial neuron networks, but also are interesting for realizing intelligent biomaterials.

Acknowledgements

This project is supported by the National Natural Science Foundation of China (Grant No.51302276) and China Postdoctoral Science Foundation Funded Project (grant number: 2014M551557).

References

1. V. M. Ho, J. A. Lee and K. C. Martin, *Science*, 2011, **334** (6056), 623.
2. G. Q. Bi and M. M. Poo, *J. Neurosci.*, 1998, **18** (24), 10464.
3. L. F. Abbott and S. B. Nelson, *Nature Neuroscience*, 2000, **3**(11), 1178.
4. G. Voglis and N. Tavernarakis, *EMBO Reports*, 2006, **7** (11), 1104.
5. A. Z. Stieg, A. V. Avizienis, H. O. Sillin, C. Martin-Olmos, M. Aono and J. K. Gimzewski, *Adv. Mater.*, 2012, **24** (2), 286.
6. L. F. Abbott and S. B. Nelson, *Nat. Neurosci.*, 2000, **3**(11), 1178.
7. S. Song, K. D. Miller and L. F. Abbott, *Nat. Neurosci.*, 2000, **3**(9), 919.

8. K. Seo, I. Kim, S. Jung, M. Jo, S. Park, J. Park, J. Shin, K. P. Biju, J. Kong, K. Lee, B. Lee and H. Hwang, *Nanotechnology*, 2011, **22** (25), 254023.
9. S. M. Yu, Y. Wu, R. Jeyasingh, D. G. Kuzum and H. S. P. Wong, *IEEE Trans. Electron Devices*, 2011, **58** (8), 2729.
10. Q. Lai, L. Zhang, Z. Li, W. F. Stickle, R. S. Williams and Y. Chen, *Adv. Mater.*, 2010, **22** (22), 2448.
11. T. Chang, S.H. Jo and W. Lu, *ACS Nano*, 2011, **5** (9), 7669.
12. F. Alibart, S. Pleutin, D. Guerin, C. Novembre, S. Lenfant, K. Lmimouni, C. Gamrat and D. Vuillaume, *Adv. Mater.*, 2010, **20** (2), 330.
13. D. Kuzum, R. G. D. Jeyasingh, B. Lee and H. S. P. Wong, *Nano Lett.*, 2012, **12** (5), 2179.
14. S. H. Jo, T. Chang, I. Ebong, B. B. Bhadviya, P. Mazumder and W. Lu, *Nano Lett.*, 2010, **10** (4), 1297.
15. T. Ohno, T. Hasegawa, T. Tsuruoka, K. Terabe, J. K. Gimzewski and M. Aono, *Nat. Mater.*, 2011, **10** (8), 591.
16. Z. Q. Wang, H.Y. Xu, X. H. Li, H. Yu, Y.C. Liu and X.J. Zhu, *Adv. Funct. Mater.*, 2012, **22** (13), 2759.
17. K. Kim, C.L. Chen, Q. Truong, A.M. Shen and Y. Chen, *Adv. Mater.*, 2013, **25** (12), 1693.
18. L. Q. Zhu, C. J. Wan, L. Q. Guo, S. Yi and Q. Wan, *Nat. Commun.*, 2014, **5**, 3158.

19. G. D. Wu, C. J. Wan, J. M. Zhou, L. Q. Zhu and Q. Wan, *Nanotechnology*, 2014, **25** (9), 094001.
20. A. A. Aldana, R. Toselli, M. C. Strumia and M. Martinelli, *J. Mater. Chem.*, 2012, **22**(42), 22670.
21. A. M. Martins, C. M. Alves, F. K. Kasper, A. G. Mikos and R. L. Reis, *J. Mater. Chem.*, 2010, **20**(9), 1638.
22. J. K. F. Suh and H. W. T. Matthew, *Biomaterials*, 2000, **21**(24), 2589.
23. I. V. Yannas, J. F. Burke, D. P. Orgill and E. M. Skrabut, *Science*, 1982, **215**(4529), 174.
24. J. A. Seo, J. H. Koh, D. K. Roh and J. H. Kim, *Solid State Ionics*, 2009, **180**(14-16), 998.
25. B. Zhou, J. Sun, X. Han, J. Jiang and Q. Wan, *IEEE Electron Device Lett.*, 2011, **32** (11), 1549.
26. W. Dou, L.Q. Zhu, J. Jiang and Q. Wan, *IEEE Electron Device Lett.*, 2013, **34** (2), 259.
27. M. Berggren, D. Nilsson and N. D. Robinson, *Nat. Mater.*, 2007, **6** (1), 3.
28. D. Tobjork and R. Osterbacka, *Adv. Mater.*, 2011, **23** (17), 1935.
29. J. J. Boland, *Nat. Mater.*, 2010, **9** (10), 790.
30. A. X. Lu, J. Sun, J. Jiang and Q. Wan, *IEEE Electron Device Letters*, 2010, **31** (10), 1137.
31. M. T. Colomer, *Adv. Mater.*, 2006, **18** (3), 371.
32. J. Brugnerotto, J. Lizardi and F. M. Goycoolea, *Polymer*, 2001, **42**(8), 3569.

33. Y. G. Jin, S. Z. Qiao, J. C. D. da Costa, B. J. Wood, B. P. Ladewig and G. Q. Lu, *Adv. Fun. Mater.*, 2007, **17** (16), 3304.
34. C. Zhong, Y. X. Deng, A. F. Roudsari, A. Kapetanovic, M. P. Anantram and M. Rolandi, *Nat. Commun.*, 2011, **2**, 476.
35. P. Barquinha, G. Goncalves, L. Pereira, R. Martins and E. Fortunato, *Thin Solid Film*, 2007, **515** (24), 8450.
36. M. E. Grubbs, M. Deal, Y. Nishi and B. M. Clemens, *IEEE Electron Device Letters*, 2009, **30** (9), 925.
37. G. Q. Bi and M. M. Poo, *J. Neurosci.*, 1998, **18**(24), 10464.
38. C. J. Wan, L. Q. Zhu, J. M. Zhou, Y. Shi and Q. Wan, *Nanoscale*, 2006, **5**(21), 10194.
39. R. S. Zucker and W. G. Regehr, *Annu. Rev. Physiol.*, 2002, **64**, 355.
40. D. V. Buonomano, *J. Neurosci.*, 2000, **20**(3), 1129.
41. E. S. Fortune and G. J. Rose, *Trends in Neurosciences*, 2001, **24**(7), 381.
42. L. F. Abbott¹ and W. G. Regehr, *Nature*, 2004, **431**(7010), 796.

Figure captions

Fig.1 (a) The schematic diagram of the coplanar-gate IZO-based synaptic transistors gated by chitosan-based proton conductors on paper substrates. (b) Cross-sectional SEM images of the chitosan-based proton conductor films on a Si substrate. Inset: cross-sectional SEM images of the chitosan-based proton conductor films on a paper substrate. (c) A photo of the bended synaptic transistor arrays on a paper substrate.

Fig. 2 (a) The mechanism of protonation process for chitosan in the acetic acid solution. (b) Cole-Cole plots of the chitosan-based proton conductor film. (c) Grotthuss mechanism for proton conduction along the hydrogen bonds formed by water and polysaccharide polar groups.

Fig. 3 Schematic structure of the coplanar-gate chitosan gating synaptic transistor and a post-synaptic current triggered by a pre-synaptic spike. (a) A scheme diagram showing a biological synapse. (b) A schematic diagram showing the synaptic transistor; (c) A symbol represents EPSC testing in the synaptic transistor (a pre-synaptic spike applied on the bottom gate triggers an EPSC on the drain). (d) EPSC triggered by a pre-synaptic spike (0.5 V, 10 ms). EPSC is measured at $V_{ds}=0.6$ V.

Fig. 4 Paired-pulse facilitation. (a) A pair of pre-synaptic spikes and the triggered EPSC under an inter-spike interval time of 200 ms. A1 and A2 represent the amplitudes of the first and second EPSCs, respectively. (b) PPF index, defined as the ratio of $A2/A1$, plotted as a function of inter-spike interval, Δt_{pre} , between the two consecutive spikes.

Fig. 5 Dynamic filter behaviors of the coplanar-gate synaptic transistor. (a) EPSCs recorded in response to stimulus train with different frequencies (1.0 Hz, 2.0 Hz, 5 Hz, 10 Hz, 20 Hz, 50Hz and 100 Hz). The stimulus train at each frequency is consisted of 10 stimulus spikes (0.5 V, 10 ms). (b) EPSCs amplitude gain (A_{10}/A_1) plotted as a function of pre-synaptic spike frequency.

Fig. 6 Spatial summation of the artificial synapse. (a) A scheme of dual coplanar-gate synaptic transistor showing spatial summation of two pre-synaptic inputs from two synapses. (b) The schematic digram of spatial summation testing. (c) EPSCs triggered by pre-synaptic spikes 1 (0.5 V, 20 ms) and pre-synaptic spikes 2 (1 V, 20 ms), respectively. (d) The amplitude of the EPSCs at $t=0$ (when the pre-synaptic spike applied on the pre-synapse 1 finished) is plotted as a function of $\Delta t_{pre2-pre1}$, between the two pre-synaptic spikes.

Fig. 1

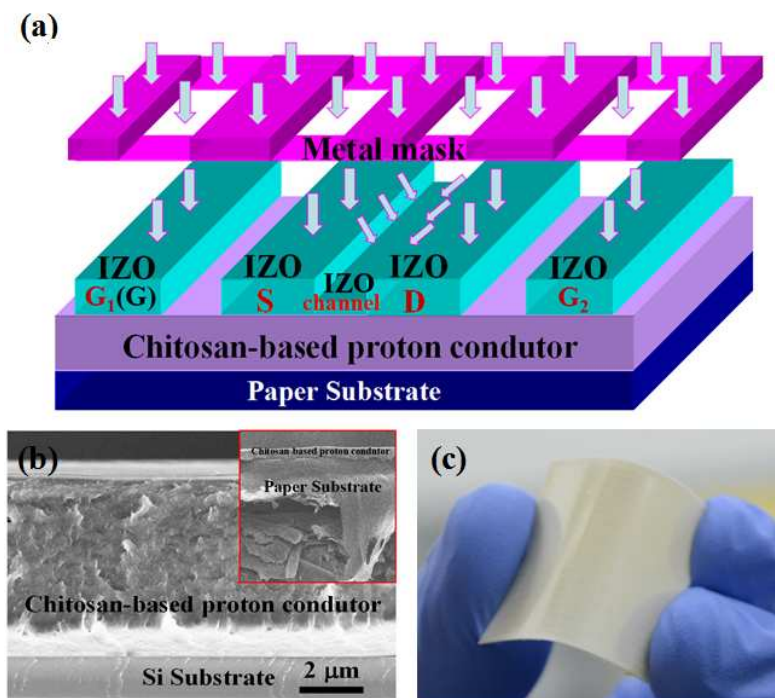


Fig. 2

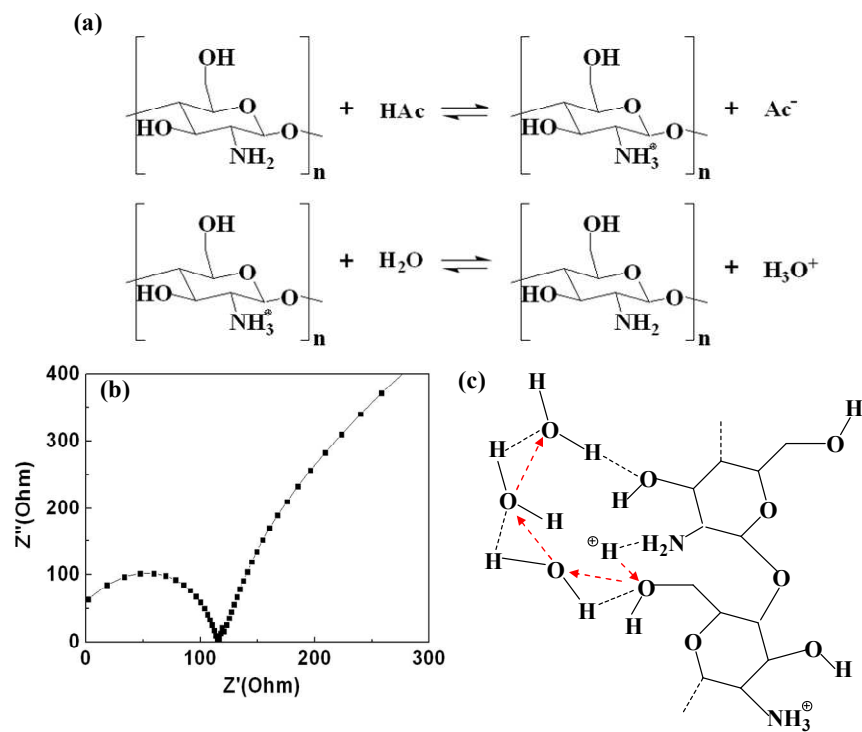


Fig. 3

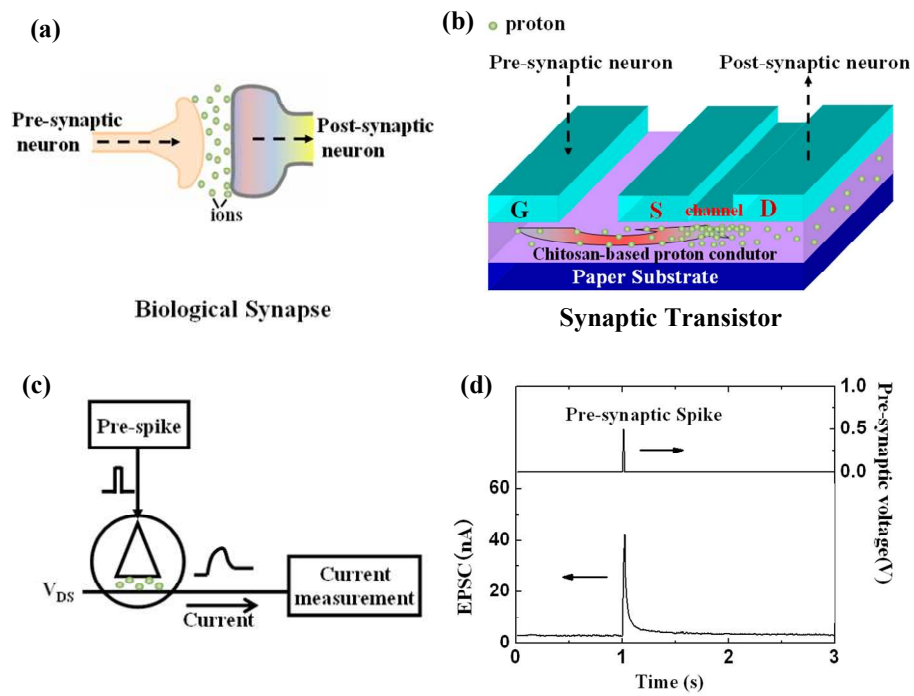


Fig. 4

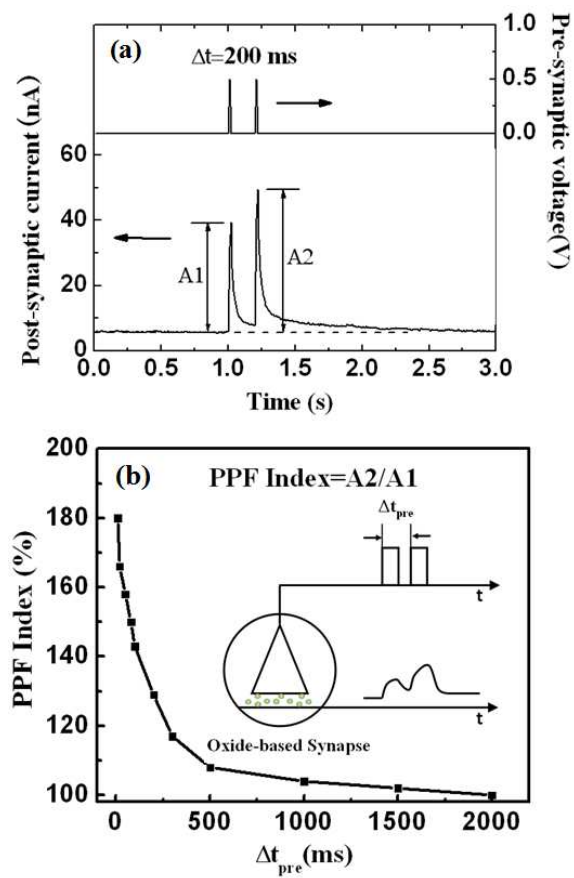


Fig.5

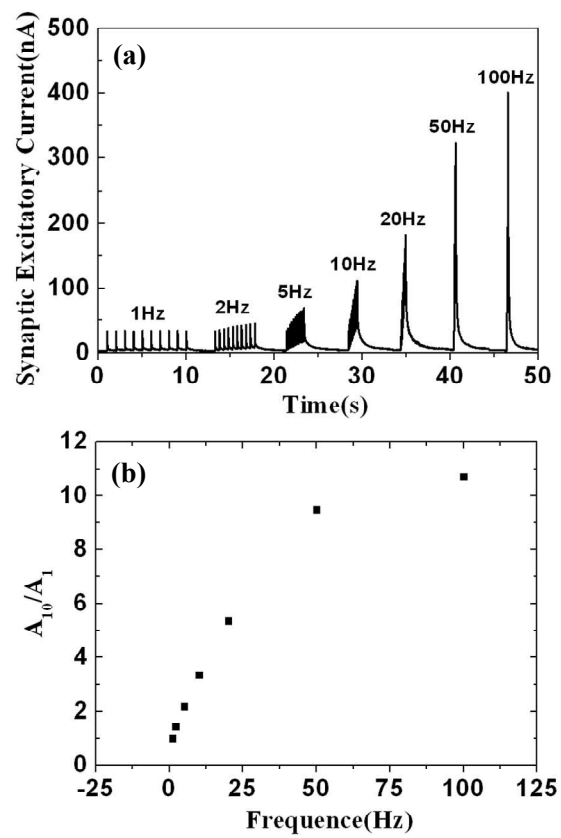


Fig. 6

